American Psychological Association

Behavioral Neuroscience

0735-7044/18/$12.00

2018, Vol. 132, No. 5, 453–468
http://dx.doi.org/10.1037/bne0000254

Neurophysiological Signatures of Temporal Coordination Between Retrosplenial Cortex and the Hippocampal Formation

Andrew S. Alexander
University of California, San Diego, and Boston University

Lara M. Rangel
University of California, San Diego

David Tingley
New York University

Douglas A. Nitz
University of California, San Diego

Retrosplenial cortex (RSC) is heavily interconnected with a multitude of cortical regions and is directly connected with the hippocampal formation. As such, it is a likely coordinator of information transfer between the hippocampus (HPC) and cortex in the service of spatial cognition and episodic memory. The current work examined three potential temporal frameworks for retrosplenial–hippocampal communication, namely, theta frequency oscillations (6–12 Hz), sharp-wave/ripple events, and repeating, theta phase-locked shifts from low (30–65 Hz) to high (120–160 Hz) gamma frequency oscillations. From simultaneous recordings of single units and local field potentials (LFPs) in RSC and HPC, we report the presence of prominent theta, low-gamma, and high-gamma oscillations in the retrosplenial LFP. Retrosplenial and hippocampal theta rhythms were strongly coherent and subgroups of retrosplenial neurons exhibited either spiking at theta frequencies and/or spike-phase-locking to theta. Retrosplenial neurons were also phase-locked to local low- and high-gamma rhythms, and power in these frequency bands was coupled in a sequential fashion to specific phases of hippocampal and retrosplenial theta rhythms. Coordinated activity between the two regions also occurred during hippocampal sharp-wave/ripple events, where retrosplenial neuron populations were modulated in their spiking and retrosplenial LFPs exhibited sharp-wave-like events that co-occurred with those observed in HPC. These results identify several temporal windows of synchronization between RSC and HPC that may mediate cortico-hippocampal processes related to learning, memory, and spatial representation.

Keywords: retrosplenial, hippocampus, theta oscillations, sharp wave ripples, gamma oscillations

The hippocampus (HPC) is crucial for spatial cognition, learning, and memory (Fortin, Agster, & Eichenbaum, 2002; Morris, Garrud, Rawlins, & O'Keefe, 1982; O'Keefe & Dostrovsky, 1971; Scoville & Milner, 1957). The retrosplenial cortex (RSC) has bidirectional connectivity with the HPC and is also implicated in spatial and mnemonic processing (Alexander & Nitz, 2015, 2017; Cho & Sharp, 2001; Cowansage et al., 2014; Czajkowski et al., 2014; Jacob et al., 2017; Keene & Bucci, 2008a, 2008b; Keene & Bucci, 2009; Pothuizen, Davies, Aggleton, & Vann, 2010; Robinson et al., 2014; Robinson, Keene, Iaccarino, Duan, & Bucci, 2011; Smith, Barredo, & Mizumori, 2012; Vann & Aggleton, 2002, 2004; Vann, Kristina Wilton, Muir, & Aggleton, 2003; Wyss & Van Groen, 1992). RSC is anatomically positioned to serve as an anatomical intermediary between the HPC and sensory, motor, and association cortices and likely influences HPC processing via excitatory projections into the entorhinal cortex (EC) and subiculum (SUB; Czajkowski et al., 2013; Olsen, Ohara, Iijima, & Witter, 2017; Van Groen & Wyss, 1990, 2003; Vogt & Miller, 1983; Wyss & Van Groen, 1992; Yamawaki, Radulovic, & Shepherd, 2016). RSC receives HPC output, both directly, and through SUB and EC. Thus, RSC-HPC circuitry may form a critical conduit for the integration of neocortical processes with those of HPC.

Despite the well-known interconnectivity of HPC and RSC, little research has examined temporal coordination of neurophysiological signals between these regions and how they might impact spatial representation and memory function. Neural oscillations have the ability to facilitate communication between interacting brain regions (Buzsáki, 2002, 2010; Fries, 2015), and the rodent HPC manifests a number of distinct oscillatory patterns that may serve to constrain interactions between HPC and other brain regions. For example, the local field potential (LFP) possesses a prominent theta rhythm (6–12 Hz) during periods of active explo-

This article was published Online First August 2, 2018.

Andrew S. Alexander, Department of Cognitive Science, University of California, San Diego, and Department of Psychological and Brain Sciences, Center for Systems Neuroscience, Boston University; Lara M. Rangel, Department of Cognitive Science, University of California; David Tingley, Neuroscience Institute, School of Medicine, New York University; Douglas A. Nitz, Department of Cognitive Science, University of California.

Correspondence concerning this article should be addressed to Andrew S. Alexander, Department of Psychological and Brain Sciences, Center for Systems Neuroscience, Boston University, 610 Commonwealth Avenue, Boston, MA 02215. E-mail: asalexan@bu.edu

ration, which is generated in part by projections arising from the medial septum and EC and is pronounced during awake mobility and REM sleep (Vanderwolf, 1969; Winson, 1974; Colom & Bland, 1987; Buzsáki, 2002). The theta rhythm temporally organizes the spiking activity of HPC neurons, a property potentially significant for the purposes of gating information flow between HPC subregions, between HPC and cortical areas, and for timing the initiation of voluntary movements (Brandon, Bogaard, Schultheiss, & Hasselmo, 2013; Buño & Velluti, 1977; Dragoi & Buzsáki, 2006; Foster & Wilson, 2007; Hyman, Zilli, Paley, & Hasselmo, 2005; Jones & Wilson, 2005; O'Keefe & Recce, 1993; Remondes & Wilson, 2013; Semba & Komisaruk, 1978; Siapas, Lubenov, & Wilson, 2005; Skaggs, McNaughton, Wilson, & Barnes, 1996). Like the HPC, RSC is innervated, albeit less densely, by EC and medial septum (Borst, Leung, & MacFabe, 1987; Vann, Aggleton, & Maguire, 2009; Wyss & Van Groen, 1992) and so is likely to exhibit theta frequency modulation of its dynamics that is coherent with that of HPC. Finally, previous experiments examining coordination of RSC and HPC theta rhythms in anesthesia and REM sleep suggest that coherence between HPC and RSC theta rhythmic spiking and LFP activity characterizes HPC/RSC interaction (Borst et al., 1987; Cho & Sharp, 2001; Colom, Christie, & Bland, 1988; Koike et al., 2017; Talk, Kang, & Gabriel, 2004).

Recent work has identified a cycling of HPC low-gamma to high-gamma frequency oscillations that is phase-locked to HPC theta-frequency LFP oscillations (Colgin et al., 2009; Koike et al., 2017). The low- and high-gamma components are thought to arise from HPC subregion CA3 and EC inputs, respectively, and appear to determine whether HPC subregion CA1 spiking activity encodes locations in the near future versus the recent past (Bieri, Bobbitt, & Colgin, 2014; Pfeiffer & Foster, 2015). Thus, an additional temporal framework for RSC-HPC coordination could result from shifts between low-gamma and high-gamma oscillations nested within the theta rhythm.

Finally, temporal coordination of RSC-HPC communication could also occur during sharp-wave/ripple events (SWRs; Buzsáki, Horváth, Urioste, Hetke, & Wise, 1992; Chrobak & Buzsáki, 1994, 1996). SWR events typically occur during awake immobility and slow-wave sleep and are composed of two components: the "sharp wave," an irregular, large amplitude, excitatory wave prominent in LFPs from HPC subregion CA1 stratum radiatum, and the "ripple," a high-frequency oscillation (150–250 Hz) that rides atop the sharp wave and is driven by synchronous firing among large populations of excitatory and inhibitory HPC neurons (Buzsáki, 2015). During SWRs, HPC pyramidal neurons exhibit sequential firing that replays the animal's previous trajectory through the environment or, conversely, predicts the future path of the animal (Diba & Buzsáki, 2007; Foster & Wilson, 2006). HPC firing activity accompanying SWRs is implicated in trajectory planning (Jadhav, Kemere, German, & Frank, 2012; Pfeiffer & Foster, 2013), as well as memory formation, consolidation, and retrieval (Jackson, Johnson, & Redish, 2006; Jadhav et al., 2012; O'Neill, Senior, Allen, Huxter, & Csicsvari, 2008; O'Neill, Senior, & Csicsvari, 2006; Singer, Carr, Karlsson, & Frank, 2013).

To determine whether RSC-HPC interaction could be supported by any or all of the three prominent modes for temporal organization of HPC spiking activity, we recorded single neuron spiking activity and LFPs from both RSC and HPC during track-running and open-field foraging in rats. We report subpopulations of RSC neurons that exhibit theta rhythmic spiking activity and/or spike-phase-locking to the HPC theta rhythm. RSC LFPs exhibited peaks in power at distinct low- and high-gamma frequencies and these gamma oscillations modulated the spike timing of RSC subpopulations. Furthermore, the amplitude of low- and high-gamma RSC LFP components exhibited cycling across phases of the theta-frequency oscillations and such cycling was temporally offset from the low-to-high-gamma cycling observed in HPC LFPs. Finally, we also report the presence of robust SWR-like events in RSC LFPs as well as RSC neuron spiking activity modulated both positively and negatively by HPC SWRs. Collectively, the results identify multiple temporal frameworks by which RSC and HPC are linked in their neurophysiological dynamics and suggest that RSC-HPC interactions play a role in a variety of spatial and mnemonic processes occurring during mobile and immobile behavioral states.

Method

Subjects

Male Long–Evans rats ($n = 4$) served as behavioral subjects and were housed individually and kept on a 12-hr light/dark cycle. Animals were habituated to the colony room and handled daily for a period of 1–2 weeks prior to training on track-running, free-foraging, or target-pursuit tasks. Rats were food restricted to approximately 85–90% of their free-fed weight. Water was available continuously. All experimental protocols adhered to Association for Assessment and Accreditation of Laboratory Animal Care guidelines and were approved by Institutional Animal Care and Use Committee and the University of California, San Diego Animal Care Program.

Behavior

Track-running paradigms. Two rats were trained to navigate around plus-, ring-, or *W*-shaped tracks for reward. The track edges ranged between 2 and 4 cm in height, which allowed the animal an unobstructed view of the full environment. Both animals ran the plus and ring tracks in the clockwise direction. One rat was trained to run half traversals in addition to the full traversals that both rats ran. This same rat was also trained to run back and forth on the *W*-shaped track for reward. Fixed spatial cues on the walls ensured consistent spatial relationships that defined the boundaries of the recording room across days. The spatial firing patterns of neurons recorded in these animals was previously reported (Alexander & Nitz, 2015, 2017).

Target-chasing paradigm. Two rats were trained to freely forage or pursue a moving light stimulus in a 1.2-m diameter circular arena for reward. The arena was placed on a table 0.9 m off of the floor. The boundaries of the arena were approximately 2.5 cm in height and there were prominent fixed distal cues on the walls of the surrounding recording room. Rats were shaped to pursue a 1.5-cm diameter light stimulus (originating from an experimenter controlled green laser pointer) for approximately 20 min per day. The temporal length of individual pursuits ranged anywhere between 0.5 and 5 s on average. During each pursuit, the goal of the animal was to "catch" the light stimulus. Following

interception, the laser would switch off and one fourth of a honey-nut Cheerio (General Mills, Minneapolis, Minnesota) would be thrown to a random position in the environment. The light stimulus would then reappear hovering near the reward to guide the animal. The number of pseudorandom pursuit paths within a session was typically between 40 and 80. Further, characteristic laser patterns were instantiated, in which the moving target would execute a stereotypical path through the arena that began and ended at the same approximate allocentric locations within the arena and recording room. These characteristic paths occurred less frequently (<20 times) than random pursuit trajectories and were randomly interspersed throughout the target-chasing block. For most sessions, the target-pursuit block occurred between free-foraging blocks (approximately 10 min each). Rats received extensive training on either track-running or target-chasing/free-exploration tasks prior to implantation of in vivo electrophysiological recording devices.

Surgery

Rats were surgically implanted with tetrode arrays (twisted sets of four 12-μm tungsten wires or 17-μm platinum-iridium, tungsten, or nickel chromium wires) fitted to custom-fabricated microdrives that allowed movement in 40-μm increments. Each microdrive contained four tetrodes. Rats were implanted with three total microdrives across RSC and HPC. Rats were anesthetized with isoflurane and positioned in a stereotaxic device (Kopf Instruments, Tujunga, CA). Following craniotomy and resection of dura mater overlying RSC, microdrives were implanted relative to bregma (anterior/posterior [A/P] −5–6.5 mm, medial/lateral [M/L] ±0.7–1.2 mm, dorsal/ventral [D/V] −0.5 mm, 10–12° medial/lateral angle). All animals additionally received a HPC microdrive targeted to the CA1 subregion (target coordinates relative to bregma, A/P −3.8 mm and M/L ±2.3 mm).

Recordings

Each microdrive had one or two electrical interface boards (EIB-16, Neuralynx, Bozeman, MT) individually connected to amplifying headstages (20×, Triangle Biosystems, Durham, NC). Signals were initially amplified and filtered (50x, 150-Hz high pass) on the way to an acquisition computer running Plexon (Dallas, TX) SortClient software. Here, the signal was digitized at 40 kHz, filtered at 0.45–9 kHz and amplified 1–15× (to reach a total of 1,000–15,000×). LFP signals were digitized at 1 KHz, bandpass filtered in the 1- to 450-Hz range, and referenced to a skull screw positioned above the cerebellum. Electrodes were moved ventrally (40 μm) between most recordings to maximize the amount of distinct units collected for each animal.

Animal position was tracked using a camera set 10 ft above the recording room floor. Plexon's CinePlex Studio software was utilized to separately detect blue and red LED lights. Lights sat approximately 4.5 cm apart and were positioned perpendicular to the length of the animal's head.

For track-running, recordings lasted approximately 45 min, the amount of time needed for the animal to complete an absolute minimum of five uninterrupted runs for plus and/or ring track conditions. For target-pursuit, recordings were on average 45 min long, the amount of time needed to acquire suitable quantities of target-pursuit trials as well as free-foraging blocks with adequate spatial coverage. Single-units were identified using Plexon OfflineSorter software. Primary waveform parameters utilized were peak height, peak–valley, energy, and principal components.

Histology

Animals were perfused with 4% paraformaldehyde under deep anesthesia. Brains were removed and sliced into 50-μm sections and Nissl-stained to identify the trajectory and depth of electrode wires in RSC and HPC. RSC was defined in accordance with our previous work (Alexander & Nitz, 2015, 2017) in the region. Dorsally, the lateral boundary of RSC was considered to be 1–2 mm lateral to the lip of the cingulate bundle. Ventrally, the lateral edge was defined by the transition from RSC to the SUB. All tetrodes were determined to be within the bounds of RSC. Documented microdrive depth across recordings and final electrode depth observed in histology were compared and found to be compatible in all cases.

Data Analysis

Power spectrum and cross-region coherence and amplitude-coupling analyses. For each recording, the power spectral density (PSD; pwelch in MATLAB) and coherence (mscohere in MATLAB) was calculated using one subjectively noise-free raw LFP from both RSC and HPC. LFPs were then band-pass filtered in MATLAB for theta (6–12 Hz), low-gamma (30–65 Hz), high-gamma (120–160 Hz), and SWR (150–250 Hz) frequencies. For the entire filtered LFP, the phase of each frequency band was estimated using a Hilbert transform (hilbert in MATLAB). To assess coupling in power for each frequency band across RSC and HPC, filtered LFPs were rectified and correlated for each animal and combination of frequencies. The aforementioned analyses were conducted during periods of mobility (speed >5 cm/s).

Phase-amplitude coupling analyses. For each recording, the phase of HPC theta was estimated using the aforementioned methods and all theta wave peaks were identified. One thousand theta peaks were randomly selected (potentially including those taken from either mobile or immobile states) and a wavelet transform (cwt in MATLAB with Order 4 Gaussian wavelet, ranging from 0 to 250 Hz) of 1,000 ms of corresponding RSC and HPC LFP was computed and then averaged across all theta peaks. To determine the significance of amplitude in low-gamma or high-gamma frequency ranges as a function of HPC theta phase, the mean power collapsed across all frequencies within either band was found and the mean angle and resultant vector length was calculated for each recording. For all 50 recordings included in this analysis, depth of theta phase modulation within each frequency band (i.e., length of mean resultant vector) was compared using a Wilcoxon's rank sum test to a distribution of *n*-matched maximum mean resultant vector values calculated from wavelet transforms of randomly shifted RSC LFP relative to HPC theta peak time points.

Spike Train Autocorrelations and Test of Intrinsic Theta Rhythmicity

For each neuron an autocorrelation of the spike train (xcorr function in MATLAB) was conducted for three movement condi-

tions: (a) all recorded spikes, (b) spikes that occurred when the animal was moving above the speed threshold (>5 cm/s), and (c) spikes that occurred when the animal was immobile. A PSD estimate (pwelch in MATLAB) was computed for the first 0.5 s of the autocorrelation. The peak within the theta frequency range (6–12 Hz) was identified (if a peak existed) and the average power was computed within 1 Hz of the theta peak. The ratio between this value and the mean of the entire power spectrum (1–500 Hz) was assessed. If the mean power within the theta frequency range was three times greater than the mean power in the entirety of the spectrum the neuron was identified as having theta rhythmicity in its spiking activity. The ratio of the mean power in the theta frequency range to the mean power in the remainder of the power spectrum was referred to as the *theta modulation ratio* and is depicted as a function of RSC subregion in Figure 2B.

Assessment of Phase-Locking to Theta, Low Gamma, and High Gamma Frequencies

For each RSC neuron, the firing rate as a function of phase within each of the aforementioned bands was calculated. Spike phase coherence was computed for the full LFP, irrespective of movement state. Phases were discretized into 10° bins and the number of spikes and total occupations for each phase bin were calculated for each neuron. Firing rate tuning curves as a function of phase were calculated by dividing the total number of spikes in each phase bin by the total amount of time that the phase bin was occupied in seconds. Calculations of mean phase and strength of tuning (i.e., mean resultant vector lengths) were computed on max-normalized tuning curves using the Circular Statistics toolbox for MATLAB (Berens, 2009). To assess whether a neuron had nonuniform phase related firing a Rayleigh test for nonuniformity was calculated. Neurons with p values less than 0.01 were determined to have significant tuning.

To test whether the proportion of neurons with significant phase tuning within the population was greater than expected by chance we decoupled phase and spike time relationships. To do this, LFP phase was circularly shifted a random amount relative to spike times and phase tuning curves were constructed and tested for nonuniformity (i.e., Rayleigh tests). This process was repeated 25 times to acquire a distribution of the proportion of RSC neurons expected to be phase coupled by chance. Neurons with mean resultant length vectors that were greater than the 95th percentile of the full distribution of mean resultants computed from temporally decoupled phase/spike vectors were determined to be strongly phase modulated and selected for more detailed analyses.

Assessment of Spatial Reliability

The spatial reliability of each RSC neuron was assessed using positional firing maps constructed from nonoverlapping epochs throughout a recording session. To generate a measure of reliability, a Spearman's correlation was calculated between these two nonoverlapping firing maps. For neurons recorded during track-running, mean firing rate vectors were constructed from odd and even numbered trials independently. For neurons recorded during open field sessions, two-dimensional firing maps for odd and even numbered minutes were calculated. For open field conditions, only spatial firing rate bins (3 cm × 3 cm) that had a minimum occupancy of 67 ms were considered. Across all recordings with free-exploration ($n = 18$) the average percentage of spatial bins that reached the occupancy threshold was 89.3 ± 4.3%. Open field spatial reliability was computed during free-exploration sessions (not target-chasing) and correlations were computed between spatial bins that reached this occupancy criterion in both odd and even minute spatial rate maps.

SWR Detection

Detection of SWRs was performed using custom MATLAB software. HPC LFPs were initially filtered within the 150–250 Hz (SWR) range. This filtered signal was then rectified and filtered again in the 0.75- to 6-Hz range to generate a power envelope of SWR frequency range power. Peaks in the resulting signal were identified, and those that were 3 *SD* greater than the average in the entire signal were extracted as potential SWR events. Next, any potential SWR events that occurred while the animal was moving at speeds greater than approximately 5 cm/s were removed, as SWRs are well known to occur during awake immobility. Finally, any SWRs that occurred within 500 ms of each other were removed from the potential SWR pool, in an effort to accurately assign spikes to single ripples as well as remove any potential reward consumption artifact erroneously classified as SWRs.

SWR Modulation

Modulation of RSC neurons by SWRs was assessed in recordings made near the HPC CA1 pyramidal cell layer where SWR detection is most accurate. For each neuron, we extracted the SWR-aligned spike rasters for 1 s centered on all SWRs within the recording. From this data, a SWR-aligned firing rate vector was computed. The same process was repeated 2,000 times, each time for data in which the spike train was circularly rotated a random fixed amount relative to SWR onset times.

SWR modulation of neuronal spiking was calculated by finding the mean squared error between activation in the 0- to 200-ms window after SWR onset in the real SWR-aligned firing rate vector and activation in the same time window averaged across all 2,000 randomizations. To attain a distribution of SWR modulation values for each neuron, the mean squared error between activation in the post-SWR window for each randomization versus the mean of all randomizations was also calculated. Neurons with real SWR modulation values that exceeded the 95th percentile of randomized SWR modulation values had significant SWR-aligned activation changes. To determine whether RSC neurons with significant SWR modulation were excited or inhibited, the SWR-aligned firing rate in the 0- to 200-ms window following SWR onset was compared to the window −500 to −100 ms preceding SWR onset. If the post-SWR window had greater firing than the pre-SWR window the neuron was classified as excited, and vice versa for the inhibited population. The only neurons excluded from the above analysis were those that had less than 25 total spikes across all SWR-aligned rasters. To assess the time course of SWR modulation, the peak or trough of SWR modulated neurons was found as the difference in milliseconds between SWR onset and the max modulation (either excitatory or inhibitory) in the SWR-aligned mean firing rate.

Results

One hundred ninety-five RSC neurons were recorded across four rats as animals performed various track-running tasks, free foraged, or pursued a moving target in an open arena. The analyses to be presented are based on single-unit activity and LFPs recorded across RSC subregions (Figure 1A, left). In all animals, simultaneous single unit and LFP recordings were also made in subregion CA1 (n = 270 neurons) of the HPC (Figure 1A, right). All simultaneous HPC and RSC LFP recordings were made in contralateral hemispheres. Consistent with previous reports, power spectral analyses computed during movement (speed >5 cm/s) revealed a prominent theta rhythm within the RSC LFP (Koike et al., 2017, mean RSC θ frequency = 8.62 Hz; Figure 1B, Figure 1C). Theta frequency oscillations were highly coherent between the HPC and RSC (Figure 1C, right). In addition to theta frequency oscillations, RSC LFP also featured two distinct gamma frequency oscillations, hereafter referred to as low- and high-gamma, that ranged from approximately 30–65 Hz and 120–160 Hz, respectively (Figure 1C, left; Figure 1B). Gamma frequency oscillations in HPC and RSC exhibited much less coherence than seen for theta frequency oscillations.

RSC Neurons Exhibit Multiple Forms of Theta Coherence

RSC is innervated by direct projections from HPC subregions CA1 and SUB as well as the septal nucleus and projection neurons in each region are known to exhibit robust theta rhythmic spiking activity. Thus, although RSC theta oscillations recorded in the LFP are potentially volume-conducted from the HPC, there stands the possibility that individual RSC neurons could be entrained by HPC theta output or a common rhythmic source, which ultimately could facilitate processes that require RSC-HPC coordination. To investigate this question, we examined the theta rhythmicity of RSC single units by computing the PSD of each neuron's spike train autocorrelation; 13.9% (n = 27/195) of autocorrelations of RSC spike trains taken across the entire recording session had power in the theta frequency range that was three times greater than the mean PSD power, and were subsequently classified as intrinsically theta rhythmic. Examples of three such neurons are given in Figure 2A. For some RSC neurons, theta rhythmic spiking was present during movement but undetectable during immobility (Figure 2C, right). The observed proportion of theta rhythmic neurons was somewhat greater in granular RSC (Rgc and Rgb) when compared to dysgranular RSC (Rd, Figure 2B, proportion θ rhythmic Rd = 10.4%, n = 5/48, Rgc = 16.1%, n = 10/62, Rgb = 14.1%, n = 12/85, Rg together = 15.0%, n = 22/147, binomial test, $p < .001$). Further, the overall depth of theta rhythmic modulation was greater in granular RSC, though this trend was not statistically significant (Figure 2B, mean θ-modulation ratio, Rd = 3.67. Rgc = 5, Rgb = 7.93, Kruskal–Wallis test, $\chi^2 = 2.21$, $p = .33$, post hoc Scheffé, all ps > .5).

In addition to theta rhythmic spiking activity, subpopulations of RSC neurons, including neurons with intrinsic theta rhythmicity,

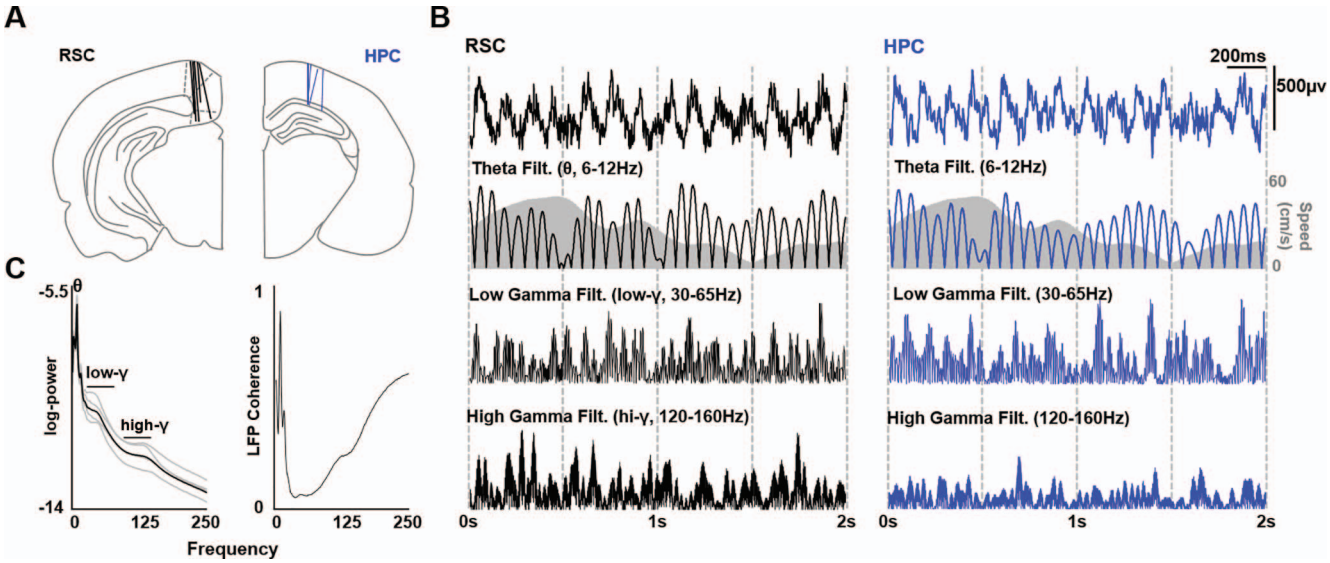

Figure 1. Electrode placements, and identification of relevant oscillatory signals in local field potentials. A. Left, placement of electrode wires across all animals in RSC collapsed across hemispheres. Right, placement of electrode wires in dorsal CA1 collapsed across hemispheres. B. First row – For the same time period, 2 seconds of raw local field potential for RSC in black and HPC in blue (in gray). Second row, rectified theta-filtered LFP from above with corresponding linear speed of the animal in gray. Third row, corresponding rectified low gamma filtered LFP. Fourth row, corresponding rectified high gamma filtered LFP. Gray dashed vertical lines delineate half-second intervals. C. Left, mean log-power spectrum across all animals and recordings in black. Mean log-power spectrum across all recordings for each animal shown as gray traces. θ, low-y, and hi-y, demarcations placed above approximate ranges of theta, low gamma, and high gamma, respectively. Right, mean coherence between RSC LFP and HPC LFP across all rats and recordings shows highest coherence in the theta frequency range. See the online article for the color version of this figure.

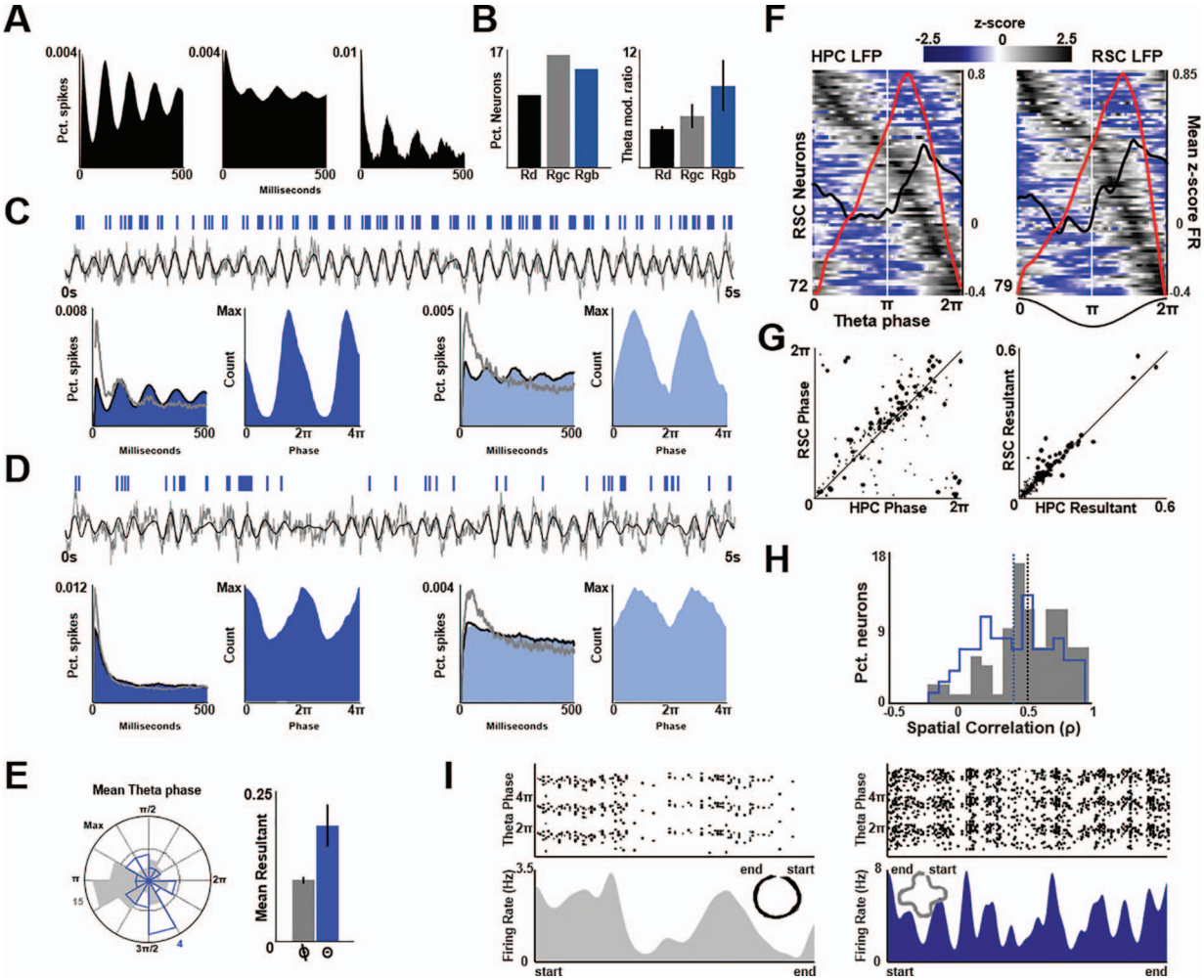

Figure 2. RSC neurons phase lock to HPC and RSC theta oscillations independent of intrinsic theta rhythmicity. A. Spike train autocorrelations of three example intrinsically theta rhythmic RSC neurons. B. Left, percent of neurons recorded in each RSC sub-region that had theta rhythmic spiking. Right, average magnitude of theta rhythmicity for neurons identified as intrinsically theta rhythmic in each region. C. Two example RSC neurons that had theta rhythmic spiking and were coupled to specific phases of the HPC theta rhythm. For each neuron, the left panel depicts the spike train autocorrelations for the whole recording (filled color), periods in which the animal was moving (in black, speed greater than 5 cm/s), and epochs in which the animal was not moving in gray. Right panels, max-normalized histogram of spike counts as a function of HPC theta phase. Spike train on top corresponds to example neuron on the left. D. Same as in Figure 2C above, but for two RSC neurons that did not have intrinsic theta rhythmic spiking yet remained coupled to specific phases of the HPC theta rhythm. E. Left, distribution of preferred theta phases for RSC neurons with non-theta-rhythmic spiking versus theta-rhythmic spiking in gray and blue (black), respectively. Right, mean magnitude of theta phase specific tuning (i.e. resultant length) for RSC neurons that were phase-locked but not intrinsically theta rhythmic versus those that were intrinsically theta rhythmic in gray and blue (black), respectively. F. Peak sorted, normalized, spike-phase histograms for RSC neurons that were strongly entrained by the HPC theta rhythm (left) and RSC theta rhythm (right). Note that these populations are largely overlapping. Black overlay, right y-axis, average z-score firing rate across all neurons shows greater activation on the ascending phase of the theta rhythm. Red (gray) overlay, right y-axis, average z-score firing rate across all HPC neurons that were strongly entrained by the HPC theta rhythm. G. Left, mean preferred HPC theta phase plotted against mean preferred RSC theta phase for all RSC neurons in black. Large dots are neurons that exhibited strong coupling to both HPC and RSC theta. Right, resultant vector length for modulation by HPC theta phase plotted against resultant vector length for modulation by RSC theta phase for all RSC neurons in black. Large dots are neurons that exhibited strong coupling to both HPC and RSC theta. H. Distribution of spatial reliability correlations for RSC neurons that are theta-phase-locked versus those that are not in blue (black) and gray, respectively. I. Spike phase versus spatial position for two RSC neurons. Top plots, spiking activity across multiple track runs plotted as a function of spatial position along the track and corresponding HPC theta phase. Bottom plots, mean linearized spatial firing rate vectors for each neuron across all track runs. Inset, tracking data for each neuron showing structure of track. See the online article for the color version of this figure.

exhibited spike-phase coupling to the theta rhythm recorded in the HPC LFP (Figure 2C). When considered across both mobile and immobile states, 75.4% of RSC neurons (n = 147/195) exhibited significantly nonuniform relationships between HPC theta phase and spiking activity (Figure 2C and 2D; Rayleigh test for nonuniformity, $p < .01$). To more conservatively quantify the proportions of neurons with strong tuning to theta phase, we identified the subset of RSC neurons that passed the nonuniformity test and also exhibited a magnitude of theta phase coherence (i.e., mean resultant length vector) greater than the 95th percentile of a distribution of magnitude values computed from repeated randomizations of the data. Resultants from randomization were computed after shifting the spike train for each neuron relative to HPC LFP theta phase 25 times. Using this more conservative approach, 36.9% (n = 72/195) of RSC neurons exhibited significant phase locking to specific phases of the HPC theta oscillation (Figure 2F, left).

Of neurons with significant HPC theta phase modulation, 22.2% (n = 16/72) also had theta rhythmic spiking activity as assessed via analysis of their spike train autocorrelations (Figure 2C). However, not all neurons with HPC theta phase coupling were theta rhythmic in their spiking activity; 77.8% (n = 56/72) of RSC neurons that were coupled to theta phase in HPC did not have significant theta rhythmicity in their spike trains (Figure 2D). The mean preferred theta phase of non-theta-rhythmic neurons was biased to the trough and ascending phase of the theta rhythm whereas theta spiking RSC neurons were coherent with later phases of the theta wave (Figure 2E, left; mean phase non-θ rhythmic = 3.41 ± 1.25 radians; mean phase θ rhythmic = 4.25 ± 1.26 radians). Theta rhythmic neurons had statistically stronger phase tuning than non-theta-rhythmic neurons that were phase modulated (Wilcoxon's rank sum test, mean θ rhythmic = 0.19, mean non-θ rhythmic = 0.10, $z = -2.35$, $p = .02$; Figure 2E, right). These findings suggest that there are potentially distinct subpopulations, rhythmic and nonrhythmic RSC neurons, capable of coordinating their activation with HPC ensembles within theta range temporal windows.

Given the coherence between RSC and HPC theta oscillations, it is perhaps of no surprise that roughly the same proportion of neurons were phase coupled to RSC theta (40.5%, n = 79/195; Figure 2F, right) and a majority of the neurons were modulated by theta phase in both regions (86.1%, n = 68/79). On average, RSC neurons fired most during the ascending phase of the theta wave (Figure 2F, overlaid black lines). Interestingly, peak RSC activation followed the maximal phasic firing of HPC neurons, suggesting that RSC activation is potentially driven by HPC output (Figure 2F, overlaid red line; mean [±*SD*] HPC θ phase of peak RSC firing = 5.76 ± 1.23 rad., mean HPC θ phase of peak HPC firing = 4.51 ± 1.10 rad., Kuiper test for difference in phase of peak firing, number hippocampus (nHPC) = 222, number Retrosplenial cortex (nRSC) = 72, k = 4,488, $p = .005$); mean RSC θ phase of peak RSC firing = 5.78 ± 1.15 radians, mean RSC θ phase of peak HPC firing = 4.71 ± 1.05 rad., Kuiper test for difference in phase of peak firing, nHPC = 226, nRSC = 79, k = 5,902, $p = .001$). For neurons that were theta locked to both RSC and HPC LFP, the mean preferred phase and tuning strength (length of mean resultant vector) were highly similar (Figure 2G, left, Kuiper two-sample test for mean phase, n = 68, mean [±*SD*] preferred RSC LFP θ phase = 3.25 ± 1.80, mean [±*SD*] preferred HPC LFP θ phase = 3.42 ± 1.66, k = 748, p = 1; Wilcoxon's rank sum test for mean resultant vector lengths, n = 68, mean [±*SD*] preferred RSC phase = 0.15 ± 0.10, mean [±*SD*] preferred HPC phase = 0.14 ± 0.09, $z = 0.98$, $p = .33$).

Theta phase-locked RSC neurons exhibited lower spatial reliability (correlation between spatial firing pattern on odd and even track-running trials or odd and even minutes in open field) than non-theta-locked neurons during track-running or open field behavior (Figure 2H, Wilcoxon's rank sum test, mean [± *SD*] Spearman's ρ for θ-locked = 0.42 ± 0.28, mean [±*SD*] Spearman's ρ for non-θ-locked = 0.53 ± 0.27; $z = 2.39$, $p = .02$). Further, theta entrained RSC neurons did not qualitatively appear to exhibit phase precession as observed for HPC place fields (Figure 2I). Nevertheless, a more formal analysis of this phenomenon is likely necessary given that RSC neurons exhibit spatially specific firing patterns, but not the discrete place fields exhibited by HPC neurons.

Theta Phase Entrains RSC Gamma Oscillations

When referenced to either the HPC or RSC LFP taken from the entire recording session, the total number of RSC neurons with statistically nonuniform relationships between theta phase and firing activity was greater than the distribution of expected proportions of neurons computed after randomly shifting the LFP phase relative to each neuron's spike train 25 times (Figure 3A). This same analysis was also conducted on the low- and high-gamma frequency components revealed in the power spectrum of the RSC LFP; 56% (n = 109/195) of RSC neurons were found to be phase locked to low-gamma frequencies (30–65 Hz) and 61% (n = 119/195) were locked to the high-gamma component (120–160 Hz) observed in the RSC LFP. Proportions of neurons with significant modulation decreased to near random levels when spiking was referenced to these frequency bands recorded in the HPC LFP (Figure 3A). The reverse pattern was observed for HPC neurons, consistent with observations that the coordination of activity in high frequency ranges is often the product of local interactions (Buzsáki & Wang, 2012). This conclusion is also supported by the lower power–power coupling between higher frequency bands versus theta oscillations recorded across RSC and HPC (Figure 3B).

RSC neurons could be both phase locked to hippocampal theta oscillations and to local low-gamma or high-gamma frequencies (65.3% of HPC theta-locked neurons were also phase-modulated by low-gamma in RSC, n = 96/147; 64.6% of HPC theta-locked neurons were also phase-modulated by high-gamma in RSC, n = 95/147). Many RSC neurons that were locked to HPC theta phase were also locked to both gamma components (47.6%, n = 70/147) suggesting that individual RSC neurons engage in multiple oscillatory processing states throughout a behavioral session and that this engagement is, in turn, organized according to HPC theta phase.

At the population level, this property of RSC neurons manifested as robust phase-amplitude coupling between theta phase and low- and high-gamma power in RSC LFPs during both mobile and immobile states (Figure 3C, top). This switch from low-gamma to high-gamma frequencies at the peak of the theta wave could be observed in raw LFP traces (Figure 3D) with the inflection point being near 100 Hz. The low-gamma range was strongly coupled to the ascending phase of the HPC theta wave (Figure 3E, top;

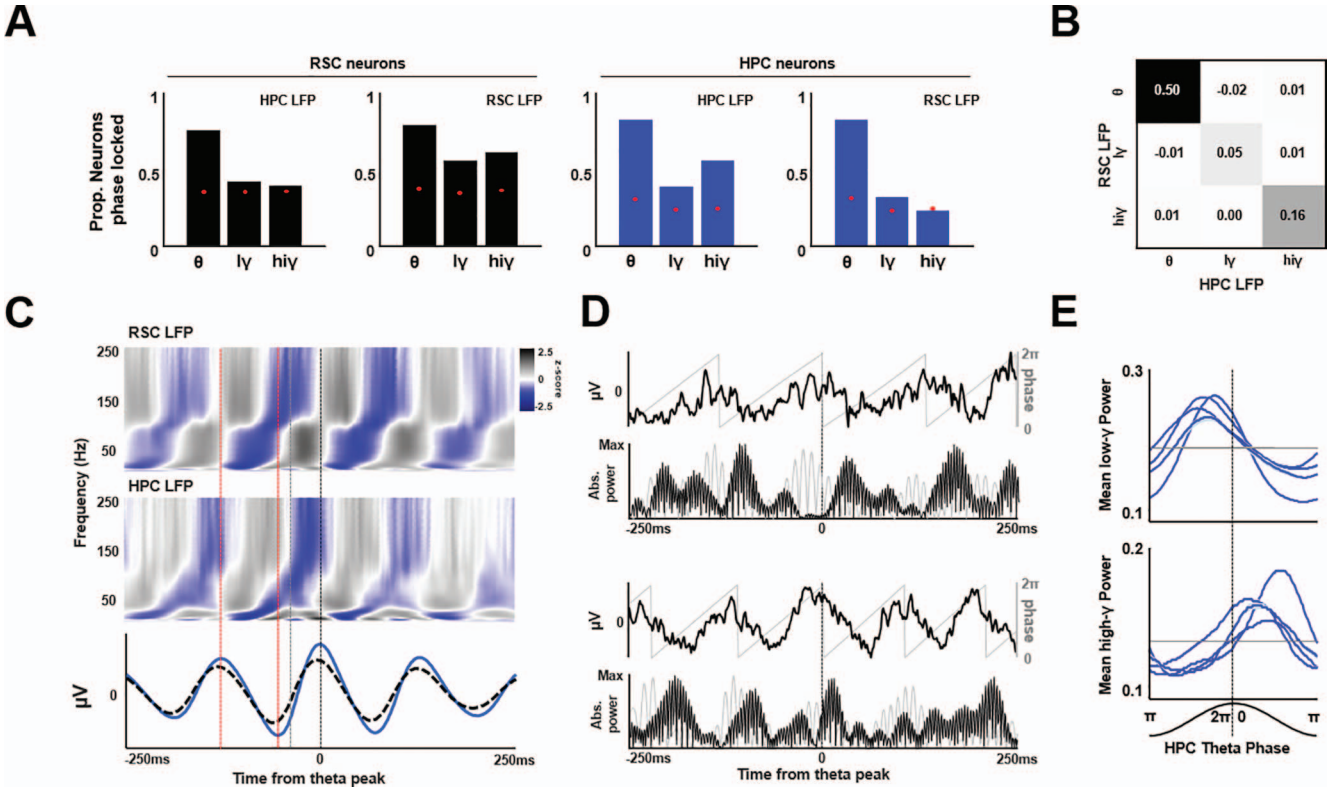

Figure 3. RSC gamma oscillations are modulated by HPC theta phase. A. Proportions of RSC neurons (in black) and HPC neurons (in blue or gray) that had significantly non-uniform relationships between spiking activity and theta (Θ), low gamma (lγ), or high gamma (hγ) phase. Red (gray) dots, mean proportion of neurons with significantly non-uniform spiking relationships to phase in the three oscillatory bands observed after circularly shifting the spike train of each neuron relative to the actual phases of each band 25 times. B. Mean correlation between power in all three frequency bands across all animals and sessions. C. Phase-amplitude coupling to HPC theta oscillations. Top, average wavelet transform across all rats and recordings of RSC LFP aligned to 1000 randomly selected HPC theta peaks shows transition between low and high gamma power occurring at the peak. Middle, average wavelet transform of HPC LFP aligned to the peak of HPC theta. Transition between low and high gamma occurs on the descending phase of theta and precedes RSC gamma patterning. For both spectrograms, each row is *z*-score normalized. Bottom, average LFP for each region for all HPC theta peaks (RSC in dashed black, HPC in solid blue or gray). Black dashed vertical line indicates approximate extracellularly recorded peak of HPC theta. Vertical dashed red (gray) lines are approximate peaks and troughs of the theta wave. Vertical gray line indicates approximate peak of HPC activity relative to theta phase. D. Two examples of transition from low to high gamma at HPC theta peaks in RSC. Top plots, 500ms of raw RSC LFP trace in black with HPC theta phase in gray. Bottom plots, corresponding rectified low and high gamma filtered LFP in gray and black respectively. Low gamma power increases before each theta peak, followed by high gamma bursts. E. Mean power in low and high gamma (top and bottom plots) frequency ranges plotted as a function of HPC theta phase. Each blue (black) line corresponds to the average for all recordings within animal. Gray lines represent same averages taken after randomly shifting the RSC and HPC LFPs relative to each other 25 times. See the online article for the color version of this figure.

μ ± *SD* HPC theta phase of peak low-gamma power = 5.00 ± 1.25 rad; Wilcoxon's rank sum test low-gamma resultants vs. *n*-matched maximum randomly shifted resultants, $n = 50$, μ ± *SD* low-γ resultant = 0.14 ± 0.05, μ ± *SD* randomized low-γ resultant = 0.02 ± 0.05, $z = -8.6$, $p < .001$). Conversely, high-gamma power was coupled to the descending phase of the theta wave (Figure 3E, bottom; μ ± *SD* of HPC theta phase of peak high-γ power = 1.21 ± 1.10 rad; Wilcoxon's rank sum test high-gamma resultants vs. n-Matched maximum randomly shifted resultants, $n = 50$, μ ± *SD* of high-γ resultants = 0.08 ± 0.03, μ ± *SD* of random high-γ resultants = 0.02 ± 0.003, $z = -8.4$, $p < .001$).

As previously reported, a similar alternation between low- and high-gamma bands relative to theta phase was observed in HPC, and occurred between lower gamma frequency ranges than observed in RSC (Figure 3C, middle panel; see also Colgin et al., 2009). The transition between gamma frequencies in HPC appeared to occur between the peak and trough of the extracellularly recorded theta wave. Almost immediately following the completion of the low to high-gamma cycle period in HPC, the RSC

exhibits a similar (and more pronounced) cycle through low to high-gamma. This suggests a potential coordination of information transfer between the two regions occurring on alternating theta cycles. The temporal relationship between alternating RSC and HPC gamma transitions appeared to match the relationship between peak firing activity as a function of theta phase observed for single HPC and RSC units (Figure 2F, left).

RSC Neurons and Local Field Potential Oscillations Are Modulated by HPC Sharp Wave Ripples (SWRs)

Entrainment of individual RSC neuron and ensemble spiking activity to the HPC theta rhythm provided evidence for synchronization between the two structures during track-running, free-foraging, and target-pursuit. However, interactions between the regions during an awake, but immobile state could be critical for processes related to trajectory planning, learning, and memory consolidation. Such processes appear to occur during HPC SWR events which tend to occur during awake immobility states and sleep. Therefore, we next sought to determine whether RSC was modulated by HPC SWRs.

We began by identifying SWR events in dorsal HPC CA1 during moments in which the animal was awake but immobile (speed <5 cm/s; Figure 4A). To assess whether SWR events in HPC modulated synaptic potentials in RSC, we averaged the RSC

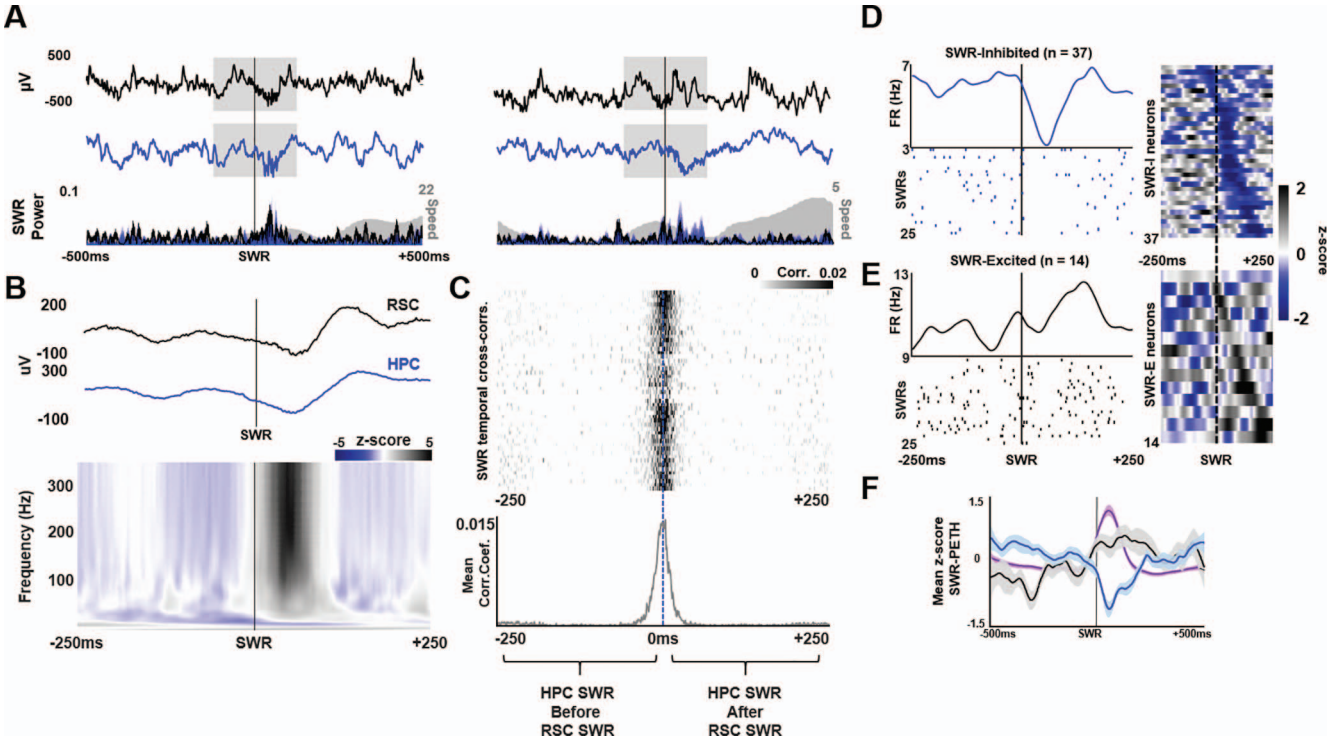

Figure 4. HPC and RSC SWRs co-occur and modulate RSC neurons. A. Raw LFP traces from both RSC (top, black) and HPC (middle, blue or gray), aligned to a detected SWR in HPC (black vertical line). Gray box is a 250ms window centered on the detected HPC SWR. Bottom, corresponding power in the SWR band for each LFP trace above. Filled gray in background and the y-axis on the right indicates the speed of the animal for the corresponding time window. B. Mean RSC (black) and HPC LFP (blue or gray) for a 500ms window surrounding all detected HPC SWRs across animals and sessions shows a pronounced sharp wave simultaneous in both structures. Bottom, average HPC-SWR-aligned wavelet transform of RSC local field potentials shows increased power in the ripple frequency range (150-250Hz) in RSC following HPC SWRs. Power in each frequency is max-normalized. C. Independently detected HPC and RSC SWRs tend to co-occur. Top plot, normalized cross-correlogram for simultaneously recorded HPC and RSC SWR onset times. Each row is the cross-correlation for an individual recording. Bottom plot, mean RSC-HPC SWR onset cross-correlation across all animals and sessions. SWRs tend to co-occur with a slight bias to the HPC SWR onset preceding RSC SWRs. D. Individual RSC neurons are inhibited by HPC SWRs. Top plot, mean SWR-triggered firing rate for an example RSC neuron that was inhibited by HPC SWRs. Lower panel, spike trains for 500ms window centered on 25 randomly selected HPC SWRs. Right panel, *z*-score normalized SWR-triggered firing rate for all SWR-inhibited RSC neurons sorted by time point of maximum inhibition following the SWR. E. Individual RSC neurons are excited by HPC SWRs. Top plot, mean SWR-triggered firing rate for an example RSC neuron that was excited by HPC SWRs. Lower panel, spike trains for 500ms window centered on 25 randomly selected HPC SWRs. Right panel, z-score normalized SWR-triggered firing rate for all SWR-excited RSC neurons sorted by time point of maximum excitation following the SWR. F. Mean SWR-aligned firing rates across all HPC (purple or gray), SWR-inhibited (blue or gray), and SWR-excited (black) populations. See the online article for the color version of this figure.

LFP triggered by the onset of HPC SWRs (Figure 4B, top). As in the average SWR-triggered HPC LFP (Figure 4B, bottom), RSC LFPs often exhibited a strong extracellular negative-going deflection reflective of the sharp wave component of the SWR that was highly synchronous with the HPC (Figure 4B, top). To determine whether the high frequency ripple component of the SWR was also evident in RSC, we computed a HPC SWR-triggered spectrogram of the RSC LFP across all rats and recordings (Figure 4B, bottom). This analysis revealed a strong power increase in the ripple frequency band (150–250 Hz) of the RSC LFP, following the onset of HPC SWRs.

Given the anatomical distance between RSC and HPC and that recordings were made in contralateral hemispheres, it is highly unlikely that the high frequency component of the SWR observed in RSC was volume conducted from the HPC. This contention is further supported by the lack of coherence between other high frequency oscillations (Figure 3A and 3B). It is possible that HPC and SUB activity during SWRs modulates local RSC circuitry via direct and indirect projections and causes cortical ripple events as recently reported in RSC and neighboring structures (Khodagholy, Gelinas, & Buzsáki, 2017). To assess whether there is a systematic lag between RSC and HPC SWR events, we next detected ripples in the RSC independently of HPC, then computed a cross-correlation of ripple onset times between the two structures (Figure 4C). On average, HPC SWRs preceded RSC SWRs ($n = 50$ recordings, mean [$\pm SD$] SWR offset $= -3.12 \pm 5.90$ ms, Wilcoxon signed-ranks test for zero median, $z = -3.61$, $p = .0003$) though in some instances, RSC SWRs appeared to precede those observed in the HPC.

If HPC SWRs reach RSC and impact the circuit, we hypothesized that there would be SWR-triggered firing rate alterations to RSC single units as observed in HPC and other cortical structures. To assess this possibility, we restricted the following analyses to those recordings in which HPC electrodes were known to lie in or near the pyramidal cell layer of HPC CA1; 32.1% of RSC neurons ($n = 51/159$) recorded under these conditions exhibited significant modulation during SWR events recorded in HPC (Figure 4D and 4E). Of RSC neurons transiently modulated, a majority were inhibited (72.5%, $n = 37/51$) in response to awake SWRs recorded in HPC (Figure 4D). In contrast, 27.5% ($n = 14/51$) were excited during SWRs, but the excitatory response was generally less pronounced than the response observed in the inhibitory population (Figure 4E). An examination of the time-course of SWR modulation revealed that SWR-excited RSC and SWR-inhibited RSC populations did not differ in their latencies to peak modulation from SWR onset, nor did either population differ from the latency to peak modulation observed in the HPC (Figure 4F, Kruskal–Wallis with post hoc Scheffé test, mean [$\pm SD$] SWR-inhibited $= 80.81 \pm 54.63$ ms; SWR-excited $= 100.21 \pm 73.77$ ms; SWR-HPC $= 77.71 \pm 46.51$ ms, $\chi^2 = 0.96$, $p = .62$, Scheffé tests all $ps > .6$).

Discussion

The current work examined the relationship between RSC single neuron spiking and LFP activity within three different temporal frameworks that characterize HPC dynamics. The frameworks are (a) HPC theta-frequency oscillations, (b) HPC SWR events, and (c) HPC LFP cycling between low- and high-gamma frequencies. The latter is itself organized by phases of HPC theta frequency oscillations. Neural dynamics in RSC were robustly related to all three temporal frameworks, pointing to the existence of multiple electrophysiological signatures of temporally coordinated interactions between the HPC and RSC.

Specifically, two populations of RSC neurons exhibited spiking activity entrained to the HPC theta rhythm, which is dominant during periods of time when the animal is awake and mobile (Vanderwolf, 1969). The first exhibited persistent rhythmic spiking similar to that observed for HPC interneuron populations (Klausberger et al., 2003; Klausberger & Somogyi, 2008), evidencing a local, direct source of theta-frequency modulation within RSC. The second population exhibited phase-locking in the absence of persistent rhythmic spiking. A second form of coordination according to theta oscillations was evident in robust phase-amplitude coupling between HPC theta phase and low- and high-gamma frequency components in the RSC. Like HPC LFPs, RSC LFPs exhibited cycling between low-gamma-dominated and high-gamma-dominated periods that were tightly ordered according to the phases of HPC LFP theta oscillations. The spiking activity of large RSC neuron subpopulations were tuned to both low- and high-gamma oscillations, and theta phases dominated by high-gamma frequencies in RSC LFPs were associated with greater RSC spiking overall. Finally, we also observed temporal coordination of RSC-HPC dynamics during immobility periods between navigational bouts. During such periods, SWRs were found to co-occur in both RSC and HPC and firing rates for many individual RSC neurons were significantly modulated. Theta-dominated mobility and SWR-dominated immobility states appear to represent distinct modes of information processing (Wilson & McNaughton, 1993; O'Keefe & Recce, 1993; Buzsáki, 2002; Jadhav et al., 2012; Pfeiffer & Foster, 2013). As such, the present observations identify behaviorally dependent signatures of RSC-HPC interaction which may ultimately serve different cognitive functions and indicate that coupling of RSC and HPC neural dynamics is common to all behavioral states.

Few studies have examined characteristics of RSC LFPs during active navigation. Consistent with previous reports, we observed a prominent theta rhythm within the RSC that was highly coherent with the HPC theta oscillation (Borst et al., 1987; Colom et al., 1988; Talk et al., 2004; Koike et al., 2017). We additionally observed two prominent gamma frequency components that were evident in all animals but lacked coherence across the two regions. The lag between RSC and HPC theta phases was minimal, at or near 0 ms for most recordings, suggesting that the observed RSC LFP theta rhythms may be volume-conducted from the HPC as has been reported for neighboring cortical regions such as posterior parietal cortex (Sirota et al., 2008). However, it is ultimately difficult to assess the local versus global sources of theta rhythmic LFP oscillations in RSC given the current experimental configuration. While volume conduction is a distinct possibility, it is also the case that the septal nucleus, thought to pace theta rhythms in HPC (Buzsáki, 2002), projects to RSC (Van Groen & Wyss, 1990, 1992, 2003; Wyss & Van Groen, 1992) and RSC neurons themselves were found to spike with theta rhythmicity tuned to both RSC and HPC LFP theta phases. Finally, prior work demonstrates that a theta rhythm can be recorded in RSC granular b (Rgb) during HPC inactivation (Talk et al., 2004).

We report that significant proportions of RSC neurons are theta entrained in their spiking, and thus, can play a role as local drivers of theta rhythmicity in RSC itself and, possibly, in cortical targets of RSC efferents. Such RSC neurons were strongly and reliably locked to HPC theta phase suggesting that they were either driven by monosynaptic connections arising in HPC and/or SUB or modulated by a shared pacemaker such as septal nucleus. An additional population of neurons was phase-locked to the HPC or RSC theta rhythm without exhibiting persistent theta-rhythmic spiking activity. In order for this to occur, these RSC neurons would likely exhibit transient theta engagement. Transient theta engagement has been observed in RSC in humans during autobiographical memory recall or memory tasks that require imagined movement through space (Foster, Kaveh, Dastjerdi, Miller, & Parvizi, 2013; Kaplan et al., 2017). Further, RSC has been shown to conditionally increase or decrease coherence with HPC, anterodorsal thalamus, or anterior cingulate theta oscillations dependent on the retrieval of recent memories (Corcoran, Frick, Radulovic, & Kay, 2016). Collectively, these results suggest that the transiently phase-locked RSC neuron populations could be important for memory recall processes.

RSC neurons were additionally phase-locked to two local gamma oscillations. Power in these gamma frequency bands was coupled to the HPC theta rhythm, indicating yet another mode by which HPC theta rhythmic output can influence cortical circuits. Specifically, the amplitude of the low-gamma component was reliably coupled to the ascending phase of the HPC theta wave. Conversely, power of the high-gamma component was maximal during the descending phase and, therefore, the transition between these two oscillations was robustly locked to HPC theta peaks. Similar gamma frequency patterning has been reported in neighboring parietal cortex (Sirota et al., 2008). A recent study reported similar phase-amplitude coupling between HPC theta and RSC gamma in RSC, but solely observed the phenomenon during REM sleep (Koike et al., 2017). Our analyses were applied to periods in which the animal was awake and actively moving when HPC theta rhythms are high in amplitude and exhibit frequency modulation as a function of running speed (Hinman, Penley, Long, Escabí, & Chrobak, 2011; Jeewajee, Barry, O'Keefe, & Burgess, 2008; Rivas, Gaztelu, & García-Austt, 1996; Sławińskaab & Kasicki, 1998). During such time periods, RSC neurons, like HPC neurons, exhibit self-motion related or spatially specific firing patterns (Alexander & Nitz, 2015, 2017; Cho & Sharp, 2001; Jacob et al., 2017; Mao, Kandler, McNaughton, & Bonin, 2017; Smith et al., 2012; Vedder, Miller, Harrison, & Smith, 2017). The stereotyped behavior and robust HPC theta rhythm may encourage the observed cross-regional phase-amplitude coupling.

We also observed coupling between HPC theta phase and HPC gamma oscillations in accordance with previous reports (Colgin et al., 2009). In HPC, low-gamma power was maximal early in the descending portion of the theta wave and high-gamma power peaked near the theta trough. Coherence between LFPs recorded in CA1 and CA3 increases during low-gamma oscillations while increased LFP coherence is observed between EC and CA1 during high-gamma oscillations (Colgin et al., 2009). These observations suggest that the gamma component is reflective of switches in information transfer between CA3 and CA1 versus EC and CA1. It is possible that the appearance of sequential low- and high-gamma rhythms in RSC reflects a similar switch between processing states, and in particular inputs. RSC receives EC output, so it is possible that the high-gamma observed there is reflective of RSC-EC processing that occurs at different theta phases relative to CA1–EC communication. RSC does not receive CA3 projections. Given this, the slow-gamma component could arise from different or changing inputs to the region, perhaps from CA1 or SUB. RSC subregions are highly interconnected so slow-gamma processing could reflect activity within a more distributed recurrent network that resembles CA3. Regardless, it is important to disentangle the sources of these gamma frequency oscillations within RSC in future work.

As the LFP was recorded extracellularly, peaks and troughs of the theta wave likely correspond to periods of synchronous hyperpolarization and depolarization across a population of neurons, respectively. This distinction becomes more concrete when examining the relationship between HPC activation and theta phase, wherein HPC neurons fire most robustly near the trough of the theta wave, presumably at their most depolarized state. RSC ensembles become active just after HPC peak activation, indicating that HPC output may ultimately cause activation in RSC circuits with each theta cycle. Coupling between RSC gamma power and theta phase is compatible with this conclusion, as a shift in the gamma oscillatory profile of RSC also initiates after the HPC theta trough and peak activation of HPC neurons.

Increases in gamma power can reflect local processing of information and the potential pacing of a network by inputs (Whittington, Traub, Kopell, Ermentrout, & Buhl, 2000). The alternating and phase offset cycling of low to high-gamma power between RSC and HPC could indicate that HPC output gates some forms of RSC processing, perhaps timing RSC integration of inputs from disparate cortical regions according to the theta cycle. Further, the RSC gamma power window is qualitatively longer in duration, transcending nearly the entire theta wave, when compared to increases in gamma amplitude observed in the HPC which span just the descending phase and trough of theta. Because RSC gamma oscillations are potentially active for a longer period of time, they overlap with roughly half of the peak HPC gamma window, which could enable the HPC to retrieve information processed in cortex during the preceding RSC gamma oscillations. Collectively, these results are consistent with the reciprocal information transfer theory of cortico-HPC communication proposed by Sirota and colleagues (Sirota et al., 2008). Given the direct and dense innervation of RSC by HPC and SUB and the presence of theta-rhythmic RSC neurons, the present findings strongly implicate RSC as a key mediator of this hypothetical process.

RSC-HPC theta rhythmic coordination during movement may subserve processes important for the spatial cognition function of the two regions. Single neurons in both HPC and RSC exhibit spatially modulated firing, wherein cells are active in response to spatial variables such as position and/or heading relative to environmental boundaries (Alexander & Nitz, 2015, 2017; Chen, Lin, Green, Barnes, & McNaughton, 1994; Cho & Sharp, 2001; Jacob et al., 2017; Knierim, Kudrimoti, & McNaughton, 1995; Muller, & Kubie, 1987; O'Keefe & Dostrovsky, 1971). Unlike the well-studied place-specific firing fields of HPC neurons (e.g., Wilson & McNaughton, 1993), RSC spatial representations are richer in that they can represent position in the environment, position within a route, repeating subcomponents of a complex route, distance within a route, or left versus right turning motion (Alexander & Nitz, 2015,

2017). It is possible that the spatially specific component of RSC spatial representations arises in the HPC or associated output structures. Alternatively, as RSC firing is correlated with spatial and behavioral variables known to flexibly modulate HPC spatial representations depending on task-demands (Ferbinteanu & Shapiro, 2003; Grieves, Wood, & Dudchenko, 2016; McNaughton, Barnes, & O'Keefe, 1983; Nitz, 2011; Save, Nerad, & Poucet, 2000; Wood, Dudchenko, Robitsek, & Eichenbaum, 2000), RSC may modulate HPC spatial representations in real time during navigation. Further, RSC is in a prime anatomical position to route visual information into the HPC, which is required for updating and stabilizing place field representations. Consistent with this contention, HPC place cells lose spatial reliability following inactivation of RSC (Cooper & Mizumori, 2001). Finally, RSC exhibits spatial responsivity that is sensitive to a combination of spatial reference frames simultaneously, indicating that the circuit may function to compute reference frame transformations of spatial positions between distinct coordinate systems (Alexander & Nitz, 2015). This capability may subserve the formation or stability of HPC spatial receptive fields which are anchored to landmarks or the geometry of the observable world (Keinath, Julian, Epstein, & Muzzio, 2017; Knierim et al., 1995; Muller & Kubie, 1987). These environmental features are necessarily encoded, at least initially, via egocentrically referenced sensory systems. Thus, HPC allocentric spatial representations (i.e., a position in the world relative to cues) require transformations from self-based spatial representations (i.e., the position of a cue relative to the animal), and this process may be supported by the RSC network (Byrne, Becker, & Burgess, 2007). It is clear that RSC processing is integrated with HPC during navigation and vice versa, and the current work indicates that this coordination may occur within theta frequency temporal windows.

Beyond the temporal framework posed by theta frequency oscillations in awake, mobile states, RSC-HPC interaction was also clearly apparent during SWR events. Recent reports have identified cortical SWR-like events that occurred in close temporal proximity to those observed in HPC, and we confirm that finding in the current dataset (Khodagholy et al., 2017). There are several issues to consider when assessing the temporal relationship between SWRs in the two structures. Mainly, there are multiple factors that make determining the actual onset of a SWR difficult. These factors primarily include the observation that SWRs can be generated locally within the HPC formation (Chrobak & Buzsáki, 1994, 1996; Patel, Schomburg, Berényi, Fujisawa, & Buzsáki, 2013; Sullivan et al., 2011), are also observed in the SUB (Chrobak & Buzsáki, 1996), a primary RSC-HPC intermediary, and that SWR events can be highly local in cortex (Khodagholy et al., 2017). Collectively, these findings make an assessment of onset time and direction of SWR "flow" complex. Nevertheless, the temporal relationship between SWR activity in HPC and RSC is consistent with previous literature examining SWR modulation in cortical regions connected to the HPC (Hahn, McFarland, Berberich, Sakmann, & Mehta, 2012; Khodagholy et al., 2017).

Given that high-frequency oscillations are only weakly coherent between RSC and HPC, the ripple component of RSC SWRs is likely generated from local cortical ensemble activity. The temporal window of single-unit activity during SWRs is consistent with spike timing dependent plasticity, and thus, comodulation during these events is thought to strengthen cell assemblies for memory formation (O'Neill et al., 2008). Consistent with this hypothesis, disruption of SWR related activity has been shown to disrupt learning and memory (Ego-Stengel & Wilson, 2010; Girardeau, Benchenane, Wiener, Buzsáki, & Zugaro, 2009; Jadhav et al., 2012). Critically, cortical ensembles in some regions exhibit SWR modulation during both slow-wave sleep and waking that appears to reactivate task-relevant information from the preceding session (Euston, Tatsuno, & McNaughton, 2007; Jadhav, Rothschild, Roumis, & Frank, 2016; Qin, McNaughton, Skaggs, & Barnes, 1997; Remondes & Wilson, 2015; Rothschild, Eban, & Frank, 2017; Wang & Ikemoto, 2016). Accordingly, activation of RSC during HPC SWRs likely reflects an important temporal window of coordination between the two regions.

The exact nature of this coordination is somewhat perplexing, as power in the ripple frequency range is typically associated with the activation of large populations of HPC neurons, whereas in the current data a majority of RSC neurons modulated by HPC SWRs were inhibited. It is possible that SWR-inhibition can be explained by GABAergic RSC interneurons receiving SWR-related excitatory input from SWR-activated CA1 and/or SUB neurons. An alternative explanation is that the observed inhibition of a subpopulation of RSC neurons during SWRs reflects the first step of a HPC-mediated disinhibition of the RSC circuitry. GABAergic projection neurons from CA1 synapse in Layer 1 of granular RSC (Rg) where they target apical dendrites of Layer 2/3 RSC pyramidal neurons (Miyashita & Rockland, 2007). RSC pyramidal cells are known to drive inhibitory interneuron networks and suppression of these cells causes disinhibition of the broader RSC circuitry (Li, Clark, Lewis, & Wilson, 2002). It is conceivable that the subpopulation of RSC neurons that are modulated during HPC SWRs receive these monosynaptic GABAergic HPC projections, and themselves typically provide excitatory drive onto local inhibitory neuron circuits. If this were the case, SWR-inhibition of this subpopulation could ultimately net a temporally offset excitation within the region.

Independent of the exact mechanisms by which HPC SWRs alter the RSC circuit, this form of synchronization could function to prime the region for integrating inputs arising in the HPC or other structures. Indeed, a subgroup of RSC neurons exhibit late-spiking properties where, following depolarizing current injections, the neuron exhibits a temporally extended depolarization ramp preceding initiation of action potentials (Kurotani et al., 2013). The prolonged synaptic integration window in this subpopulation of RSC neurons has been hypothesized to be potentially critical for associating temporally distinct sequences of stimuli for the purposes of memory or spatial navigation. Future work should assess whether these late-spiking neurons are modulated during HPC SWRs, and if so, in what manner.

It is probable that coordination of the RSC-HPC circuitry during SWRs supports mnemonic processes as in other cortico-HPC circuits. In rats and humans, damage to RSC leads to disorders of spatial navigation, but also dysfunction of contextual, spatial, associative, and sequential learning and memory (Keene & Bucci, 2008a, 2008b, 2009; Robinson et al., 2011; Valenstein et al., 1987). The EC, HPC, and RSC all exhibit atrophy and hypometabolism early in the progression of Alzheimer's disease and related pathologies (e.g., mild cognitive impairment; Devanand et al., 2007; Price et al., 2001; Valenstein et al., 1987). Activation of cell assemblies in both regions is required for learning and recall,

and there is evidence to suggest that memories can be initially encoded in RSC, retrieved from RSC, or consolidated in the cortical region following HPC processing (Cowansage et al., 2014; Czajkowski et al., 2014; Kitamura, Ogawa, Roy, et al., 2017). Here, we identify multiple frameworks of temporal coordination between the HPC and RSC, at the resolution of theta oscillations, gamma oscillations, and SWR events, that occur across behavioral states. Accordingly, future investigation is needed to identify potential roles for these specific synchronization windows in mnemonic and/or spatial processing.

References

Alexander, A. S., & Nitz, D. A. (2015). Retrosplenial cortex maps the conjunction of internal and external spaces. *Nature Neuroscience, 18,* 1143–1151. http://dx.doi.org/10.1038/nn.4058

Alexander, A. S., & Nitz, D. A. (2017). Spatially periodic activation patterns of retrosplenial cortex encode route sub-spaces and distance traveled. *Current Biology, 27,* 1551–1560. http://dx.doi.org/10.1016/j.cub.2017.04.036

Berens, P. (2009). CircStat: A MATLAB toolbox for circular statistics. *Journal of Statistical Software, 31,* 1–21. http://dx.doi.org/10.18637/jss.v031.i10

Bieri, K. W., Bobbitt, K. N., & Colgin, L. L. (2014). Slow and fast γ rhythms coordinate different spatial coding modes in hippocampal place cells. *Neuron, 82,* 670–681. http://dx.doi.org/10.1016/j.neuron.2014.03.013

Borst, J. G., Leung, L. W., & MacFabe, D. F. (1987). Electrical activity of the cingulate cortex: II. Cholinergic modulation. *Brain Research, 407,* 81–93. http://dx.doi.org/10.1016/0006-8993(87)91221-2

Brandon, M. P., Bogaard, A. R., Schultheiss, N. W., & Hasselmo, M. E. (2013). Segregation of cortical head direction cell assemblies on alternating θ cycles. *Nature Neuroscience, 16,* 739–748. http://dx.doi.org/10.1038/nn.3383

Buño, W., Jr., & Velluti, J. C. (1977). Relationships of hippocampal theta cycles with bar pressing during self-stimulation. *Physiology & Behavior, 19,* 615–621. http://dx.doi.org/10.1016/0031-9384(77)90035-X

Buzsáki, G. (2002). Theta oscillations in the hippocampus. *Neuron, 33,* 325–340. http://dx.doi.org/10.1016/S0896-6273(02)00586-X

Buzsáki, G. (2010). Neural syntax: Cell assemblies, synapsembles, and readers. *Neuron, 68,* 362–385. http://dx.doi.org/10.1016/j.neuron.2010.09.023

Buzsáki, G. (2015). Hippocampal sharp wave-ripple: A cognitive biomarker for episodic memory and planning. *Hippocampus, 25,* 1073–1188. http://dx.doi.org/10.1002/hipo.22488

Buzsáki, G., Horváth, Z., Urioste, R., Hetke, J., & Wise, K. (1992). High-frequency network oscillation in the hippocampus. *Science, 256,* 1025–1027. http://dx.doi.org/10.1126/science.1589772

Buzsáki, G., & Wang, X. J. (2012). Mechanisms of gamma oscillations. *Annual Review of Neuroscience, 35,* 203–225.

Byrne, P., Becker, S., & Burgess, N. (2007). Remembering the past and imagining the future: A neural model of spatial memory and imagery. *Psychological Review, 114,* 340–375. http://dx.doi.org/10.1037/0033-295X.114.2.340

Chen, L. L., Lin, L. H., Green, E. J., Barnes, C. A., & McNaughton, B. L. (1994). Head-direction cells in the rat posterior cortex: I. Anatomical distribution and behavioral modulation. *Experimental Brain Research, 101,* 8–23. http://dx.doi.org/10.1007/BF00243212

Cho, J., & Sharp, P. E. (2001). Head direction, place, and movement correlates for cells in the rat retrosplenial cortex. *Behavioral Neuroscience, 115,* 3–25. http://dx.doi.org/10.1037/0735-7044.115.1.3

Chrobak, J. J., & Buzsáki, G. (1994). Selective activation of deep layer (V-VI) retrohippocampal cortical neurons during hippocampal sharp waves in the behaving rat. *The Journal of Neuroscience, 14,* 6160–6170. http://dx.doi.org/10.1523/JNEUROSCI.14-10-06160.1994

Chrobak, J. J., & Buzsáki, G. (1996). High-frequency oscillations in the output networks of the hippocampal-entorhinal axis of the freely behaving rat. *The Journal of Neuroscience, 16,* 3056–3066. http://dx.doi.org/10.1523/JNEUROSCI.16-09-03056.1996

Colgin, L. L., Denninger, T., Fyhn, M., Hafting, T., Bonnevie, T., Jensen, O., . . . Moser, E. I. (2009). Frequency of gamma oscillations routes flow of information in the hippocampus. *Nature, 462,* 353–357. http://dx.doi.org/10.1038/nature08573

Colom, L. V., & Bland, B. H. (1987). State-dependent spike train dynamics of hippocampal formation neurons: Evidence for theta-on and theta-off cells. *Brain Research, 422,* 277–286. http://dx.doi.org/10.1016/0006-8993(87)90934-6

Colom, L. V., Christie, B. R., & Bland, B. H. (1988). Cingulate cell discharge patterns related to hippocampal EEG and their modulation by muscarinic and nicotinic agents. *Brain Research, 460,* 329–338. http://dx.doi.org/10.1016/0006-8993(88)90377-0

Cooper, B. G., & Mizumori, S. J. (2001). Temporary inactivation of the retrosplenial cortex causes a transient reorganization of spatial coding in the hippocampus. *The Journal of Neuroscience, 21,* 3986–4001. http://dx.doi.org/10.1523/JNEUROSCI.21-11-03986.2001

Corcoran, K. A., Frick, B. J., Radulovic, J., & Kay, L. M. (2016). Analysis of coherent activity between retrosplenial cortex, hippocampus, thalamus, and anterior cingulate cortex during retrieval of recent and remote context fear memory. *Neurobiology of Learning and Memory, 127,* 93–101. http://dx.doi.org/10.1016/j.nlm.2015.11.019

Cowansage, K. K., Shuman, T., Dillingham, B. C., Chang, A., Golshani, P., & Mayford, M. (2014). Direct reactivation of a coherent neocortical memory of context. *Neuron, 84,* 432–441. http://dx.doi.org/10.1016/j.neuron.2014.09.022

Czajkowski, R., Jayaprakash, B., Wiltgen, B., Rogerson, T., Guzman-Karlsson, M. C., Barth, A. L., . . . Silva, A. J. (2014). Encoding and storage of spatial information in the retrosplenial cortex. *Proceedings of the National Academy of Sciences of the United States of America, 111,* 8661–8666. http://dx.doi.org/10.1073/pnas.1313222111

Czajkowski, R., Sugar, J., Zhang, S. J., Couey, J. J., Ye, J., & Witter, M. P. (2013). Superficially projecting principal neurons in layer V of medial entorhinal cortex in the rat receive excitatory retrosplenial input. *The Journal of Neuroscience, 33,* 15779–15792. http://dx.doi.org/10.1523/JNEUROSCI.2646-13.2013

Devanand, D. P., Pradhaban, G., Liu, X., Khandji, A., De Santi, S., Segal, S., . . . de Leon, M. J. (2007). Hippocampal and entorhinal atrophy in mild cognitive impairment: Prediction of Alzheimer disease. *Neurology, 68,* 828–836. http://dx.doi.org/10.1212/01.wnl.0000256697.20968.d7

Diba, K., & Buzsáki, G. (2007). Forward and reverse hippocampal place-cell sequences during ripples. *Nature Neuroscience, 10,* 1241–1242. http://dx.doi.org/10.1038/nn1961

Dragoi, G., & Buzsáki, G. (2006). Temporal encoding of place sequences by hippocampal cell assemblies. *Neuron, 50,* 145–157. http://dx.doi.org/10.1016/j.neuron.2006.02.023

Ego-Stengel, V., & Wilson, M. A. (2010). Disruption of ripple-associated hippocampal activity during rest impairs spatial learning in the rat. *Hippocampus, 20,* 1–10.

Euston, D. R., Tatsuno, M., & McNaughton, B. L. (2007). Fast-forward playback of recent memory sequences in prefrontal cortex during sleep. *Science, 318,* 1147–1150. http://dx.doi.org/10.1126/science.1148979

Ferbinteanu, J., & Shapiro, M. L. (2003). Prospective and retrospective memory coding in the hippocampus. *Neuron, 40,* 1227–1239. http://dx.doi.org/10.1016/S0896-6273(03)00752-9

Fortin, N. J., Agster, K. L., & Eichenbaum, H. B. (2002). Critical role of the hippocampus in memory for sequences of events. *Nature Neuroscience, 5,* 458–462. http://dx.doi.org/10.1038/nn834

Foster, B. L., Kaveh, A., Dastjerdi, M., Miller, K. J., & Parvizi, J. (2013). Human retrosplenial cortex displays transient theta phase locking with medial temporal cortex prior to activation during autobiographical mem-

ory retrieval. *The Journal of Neuroscience, 33,* 10439–10446. http://dx.doi.org/10.1523/JNEUROSCI.0513-13.2013

Foster, D. J., & Wilson, M. A. (2006). Reverse replay of behavioural sequences in hippocampal place cells during the awake state. *Nature, 440,* 680–683. http://dx.doi.org/10.1038/nature04587

Foster, D. J., & Wilson, M. A. (2007). Hippocampal theta sequences. *Hippocampus, 17,* 1093–1099. http://dx.doi.org/10.1002/hipo.20345

Fries, P. (2015). Rhythms for cognition: Communication through coherence. *Neuron, 88,* 220–235. http://dx.doi.org/10.1016/j.neuron.2015.09.034

Girardeau, G., Benchenane, K., Wiener, S. I., Buzsáki, G., & Zugaro, M. B. (2009). Selective suppression of hippocampal ripples impairs spatial memory. *Nature Neuroscience, 12,* 1222–1223. http://dx.doi.org/10.1038/nn.2384

Grieves, R. M., Wood, E. R., & Dudchenko, P. A. (2016). Place cells on a maze encode routes rather than destinations. *eLife, 5,* e15986. http://dx.doi.org/10.7554/eLife.15986

Hahn, T. T., McFarland, J. M., Berberich, S., Sakmann, B., & Mehta, M. R. (2012). Spontaneous persistent activity in entorhinal cortex modulates cortico-hippocampal interaction in vivo. *Nature Neuroscience, 15,* 1531–1538. http://dx.doi.org/10.1038/nn.3236

Hinman, J. R., Penley, S. C., Long, L. L., Escabí, M. A., & Chrobak, J. J. (2011). Septotemporal variation in dynamics of theta: Speed and habituation. *Journal of Neurophysiology, 105,* 2675–2686. http://dx.doi.org/10.1152/jn.00837.2010

Hyman, J. M., Zilli, E. A., Paley, A. M., & Hasselmo, M. E. (2005). Medial prefrontal cortex cells show dynamic modulation with the hippocampal theta rhythm dependent on behavior. *Hippocampus, 15,* 739–749. http://dx.doi.org/10.1002/hipo.20106

Jackson, J. C., Johnson, A., & Redish, A. D. (2006). Hippocampal sharp waves and reactivation during awake states depend on repeated sequential experience. *The Journal of Neuroscience, 26,* 12415–12426. http://dx.doi.org/10.1523/JNEUROSCI.4118-06.2006

Jacob, P. Y., Casali, G., Spieser, L., Page, H., Overington, D., & Jeffery, K. (2017). An independent, landmark-dominated head-direction signal in dysgranular retrosplenial cortex. *Nature Neuroscience, 20,* 173–175. http://dx.doi.org/10.1038/nn.4465

Jadhav, S. P., Kemere, C., German, P. W., & Frank, L. M. (2012). Awake hippocampal sharp-wave ripples support spatial memory. *Science, 336,* 1454–1458. http://dx.doi.org/10.1126/science.1217230

Jadhav, S. P., Rothschild, G., Roumis, D. K., & Frank, L. M. (2016). Coordinated excitation and inhibition of prefrontal ensembles during awake hippocampal sharp-wave ripple events. *Neuron, 90,* 113–127. http://dx.doi.org/10.1016/j.neuron.2016.02.010

Jeewajee, A., Barry, C., O'Keefe, J., & Burgess, N. (2008). Grid cells and theta as oscillatory interference: Electrophysiological data from freely moving rats. *Hippocampus, 18,* 1175–1185. http://dx.doi.org/10.1002/hipo.20510

Jones, M. W., & Wilson, M. A. (2005). Theta rhythms coordinate hippocampal-prefrontal interactions in a spatial memory task. *PLoS Biology, 3,* e402. http://dx.doi.org/10.1371/journal.pbio.0030402

Kaplan, R., Bush, D., Bisby, J. A., Horner, A. J., Meyer, S. S., & Burgess, N. (2017). Medial prefrontal-medial temporal theta phase coupling in dynamic spatial imagery. *Journal of Cognitive Neuroscience, 29,* 507–519. http://dx.doi.org/10.1162/jocn_a_01064

Keene, C. S., & Bucci, D. J. (2008a). Involvement of the retrosplenial cortex in processing multiple conditioned stimuli. *Behavioral Neuroscience, 122,* 651–658. http://dx.doi.org/10.1037/0735-7044.122.3.651

Keene, C. S., & Bucci, D. J. (2008b). Neurotoxic lesions of retrosplenial cortex disrupt signaled and unsignaled contextual fear conditioning. *Behavioural Neurology, 122,* 1070–1077. http://dx.doi.org/10.1037/a0012895

Keene, C. S., & Bucci, D. J. (2009). Damage to the retrosplenial cortex produces specific impairments in spatial working memory. *Neurobiology of Learning and Memory, 91,* 408–414. http://dx.doi.org/10.1016/j.nlm.2008.10.009

Keinath, A. T., Julian, J. B., Epstein, R. A., & Muzzio, I. A. (2017). Environmental geometry aligns the hippocampal map during spatial reorientation. *Current Biology, 27,* 309–317. http://dx.doi.org/10.1016/j.cub.2016.11.046

Khodagholy, D., Gelinas, J. N., & Buzsáki, G. (2017). Learning-enhanced coupling between ripple oscillations in association cortices and hippocampus. *Science, 358,* 369–372. http://dx.doi.org/10.1126/science.aan6203

Kitamura, T., Ogawa, S. K., Roy, D. S., Okuyama, T., Morrissey, M. D., Smith, L. M., . . . Tonegawa, S. (2017). Engrams and circuits crucial for systems consolidation of a memory. *Science, 356,* 73–78. http://dx.doi.org/10.1126/science.aam6808

Klausberger, T., Magill, P. J., Márton, L. F., Roberts, J. D. B., Cobden, P. M., Buzsáki, G., & Somogyi, P. (2003). Brain-state- and cell-type-specific firing of hippocampal interneurons in vivo. *Nature, 421,* 844–848. http://dx.doi.org/10.1038/nature01374

Klausberger, T., & Somogyi, P. (2008). Neuronal diversity and temporal dynamics: The unity of hippocampal circuit operations. *Science, 321,* 53–57. http://dx.doi.org/10.1126/science.1149381

Knierim, J. J., Kudrimoti, H. S., & McNaughton, B. L. (1995). Place cells, head direction cells, and the learning of landmark stability. *The Journal of Neuroscience, 15,* 1648–1659. http://dx.doi.org/10.1523/JNEUROSCI.15-03-01648.1995

Koike, B. D. V., Farias, K. S., Billwiller, F., Almeida-Filho, D., Libourel, P. A., Tiran-Cappello, A., . . . Queiroz, C. M. (2017). Electrophysiological evidence that the retrosplenial cortex displays a strong and specific activation phased with hippocampal theta during paradoxical (REM) sleep. *The Journal of Neuroscience, 37,* 8003–8013. http://dx.doi.org/10.1523/JNEUROSCI.0026-17.2017

Kurotani, T., Miyashita, T., Wintzer, M., Konishi, T., Sakai, K., Ichinohe, N., & Rockland, K. S. (2013). Pyramidal neurons in the superficial layers of rat retrosplenial cortex exhibit a late-spiking firing property. *Brain Structure & Function, 218,* 239–254. http://dx.doi.org/10.1007/s00429-012-0398-1

Li, Q., Clark, S., Lewis, D. V., & Wilson, W. A. (2002). NMDA receptor antagonists disinhibit rat posterior cingulate and retrosplenial cortices: A potential mechanism of neurotoxicity. *The Journal of Neuroscience, 22,* 3070–3080. http://dx.doi.org/10.1523/JNEUROSCI.22-08-03070.2002

Mao, D., Kandler, S., McNaughton, B. L., & Bonin, V. (2017). Sparse orthogonal population representation of spatial context in the retrosplenial cortex. *Nature Communications, 8,* 243. http://dx.doi.org/10.1038/s41467-017-00180-9

McNaughton, B. L., Barnes, C. A., & O'Keefe, J. (1983). The contributions of position, direction, and velocity to single unit activity in the hippocampus of freely-moving rats. *Experimental Brain Research, 52,* 41–49. http://dx.doi.org/10.1007/BF00237147

Miyashita, T., & Rockland, K. S. (2007). GABAergic projections from the hippocampus to the retrosplenial cortex in the rat. *The European Journal of Neuroscience, 26,* 1193–1204. http://dx.doi.org/10.1111/j.1460-9568.2007.05745.x

Morris, R. G. M., Garrud, P., Rawlins, J. N., & O'Keefe, J. (1982). Place navigation impaired in rats with hippocampal lesions. *Nature, 297,* 681–683. http://dx.doi.org/10.1038/297681a0

Muller, R. U., & Kubie, J. L. (1987). The effects of changes in the environment on the spatial firing of hippocampal complex-spike cells. *The Journal of Neuroscience, 7,* 1951–1968. http://dx.doi.org/10.1523/JNEUROSCI.07-07-01951.1987

Nitz, D. A. (2011). Path shape impacts the extent of CA1 pattern recurrence both within and across environments. *Journal of Neurophysiology, 105,* 1815–1824. http://dx.doi.org/10.1152/jn.00573.2010

O'Keefe, J., & Dostrovsky, J. (1971). The hippocampus as a spatial map. Preliminary evidence from unit activity in the freely-moving rat. *Brain Research, 34,* 171–175. http://dx.doi.org/10.1016/0006-8993(71)90358-1

O'Keefe, J., & Recce, M. L. (1993). Phase relationship between hippocampal place units and the EEG theta rhythm. *Hippocampus, 3,* 317–330. http://dx.doi.org/10.1002/hipo.450030307

Olsen, G. M., Ohara, S., Iijima, T., & Witter, M. P. (2017). Parahippocampal and retrosplenial connections of rat posterior parietal cortex. *Hippocampus, 27,* 335–358. http://dx.doi.org/10.1002/hipo.22701

O'Neill, J., Senior, T. J., Allen, K., Huxter, J. R., & Csicsvari, J. (2008). Reactivation of experience-dependent cell assembly patterns in the hippocampus. *Nature Neuroscience, 11,* 209–215. http://dx.doi.org/10.1038/nn2037

O'Neill, J., Senior, T., & Csicsvari, J. (2006). Place-selective firing of CA1 pyramidal cells during sharp wave/ripple network patterns in exploratory behavior. *Neuron, 49,* 143–155. http://dx.doi.org/10.1016/j.neuron.2005.10.037

Patel, J., Schomburg, E. W., Berényi, A., Fujisawa, S., & Buzsáki, G. (2013). Local generation and propagation of ripples along the septotemporal axis of the hippocampus. *The Journal of Neuroscience, 33,* 17029–17041. http://dx.doi.org/10.1523/JNEUROSCI.2036-13.2013

Pfeiffer, B. E., & Foster, D. J. (2013). Hippocampal place-cell sequences depict future paths to remembered goals. *Nature, 497,* 74–79. http://dx.doi.org/10.1038/nature12112

Pfeiffer, B. E., & Foster, D. J. (2015). PLACE CELLS. Autoassociative dynamics in the generation of sequences of hippocampal place cells. *Science, 349,* 180–183. http://dx.doi.org/10.1126/science.aaa9633

Pothuizen, H. H., Davies, M., Aggleton, J. P., & Vann, S. D. (2010). Effects of selective granular retrosplenial cortex lesions on spatial working memory in rats. *Behavioural Brain Research, 208,* 566–575. http://dx.doi.org/10.1016/j.bbr.2010.01.001

Price, J. L., Ko, A. I., Wade, M. J., Tsou, S. K., McKeel, D. W., & Morris, J. C. (2001). Neuron number in the entorhinal cortex and CA1 in preclinical Alzheimer disease. *Archives of Neurology, 58,* 1395–1402. http://dx.doi.org/10.1001/archneur.58.9.1395

Qin, Y. L., McNaughton, B. L., Skaggs, W. E., & Barnes, C. A. (1997). Memory reprocessing in corticocortical and hippocampocortical neuronal ensembles. *Philosophical Transactions of the Royal Society of London Series B, Biological Sciences, 352,* 1525–1533. http://dx.doi.org/10.1098/rstb.1997.0139

Remondes, M., & Wilson, M. A. (2013). Cingulate-hippocampus coherence and trajectory coding in a sequential choice task. *Neuron, 80,* 1277–1289. http://dx.doi.org/10.1016/j.neuron.2013.08.037

Remondes, M., & Wilson, M. A. (2015). Slow-γ rhythms coordinate cingulate cortical responses to hippocampal sharp-wave ripples during wakefulness. *Cell Reports, 13,* 1327–1335. http://dx.doi.org/10.1016/j.celrep.2015.10.005

Rivas, J., Gaztelu, J. M., & García-Austt, E. (1996). Changes in hippocampal cell discharge patterns and theta rhythm spectral properties as a function of walking velocity in the guinea pig. *Experimental Brain Research, 108,* 113–118. http://dx.doi.org/10.1007/BF00242908

Robinson, S., Keene, C. S., Iaccarino, H. F., Duan, D., & Bucci, D. J. (2011). Involvement of retrosplenial cortex in forming associations between multiple sensory stimuli. *Behavioural Neurology, 125,* 578–587. http://dx.doi.org/10.1037/a0024262

Robinson, S., Todd, T. P., Pasternak, A. R., Luikart, B. W., Skelton, P. D., Urban, D. J., & Bucci, D. J. (2014). Chemogenetic silencing of neurons in retrosplenial cortex disrupts sensory preconditioning. *The Journal of Neuroscience, 34,* 10982–10988. http://dx.doi.org/10.1523/JNEUROSCI.1349-14.2014

Rothschild, G., Eban, E., & Frank, L. M. (2017). A cortical-hippocampal-cortical loop of information processing during memory consolidation. *Nature Neuroscience, 20,* 251–259.

Save, E., Nerad, L., & Poucet, B. (2000). Contribution of multiple sensory information to place field stability in hippocampal place cells. *Hippocampus, 10,* 64–76. http://dx.doi.org/10.1002/(SICI)1098-1063(2000)10:1<64::AID-HIPO7>3.0.CO;2-Y

Scoville, W. B., & Milner, B. (1957). Loss of recent memory after bilateral hippocampal lesions. *Journal of Neurology, Neurosurgery, and Psychiatry, 20,* 11–21. http://dx.doi.org/10.1136/jnnp.20.1.11

Semba, K., & Komisaruk, B. R. (1978). Phase of the theta wave in relation to different limb movements in awake rats. *Electroencephalography and Clinical Neurophysiology, 44,* 61–71. http://dx.doi.org/10.1016/0013-4694(78)90105-0

Siapas, A. G., Lubenov, E. V., & Wilson, M. A. (2005). Prefrontal phase locking to hippocampal theta oscillations. *Neuron, 46,* 141–151. http://dx.doi.org/10.1016/j.neuron.2005.02.028

Singer, A. C., Carr, M. F., Karlsson, M. P., & Frank, L. M. (2013). Hippocampal SWR activity predicts correct decisions during the initial learning of an alternation task. *Neuron, 77,* 1163–1173. http://dx.doi.org/10.1016/j.neuron.2013.01.027

Sirota, A., Montgomery, S., Fujisawa, S., Isomura, Y., Zugaro, M., & Buzsáki, G. (2008). Entrainment of neocortical neurons and gamma oscillations by the hippocampal theta rhythm. *Neuron, 60,* 683–697. http://dx.doi.org/10.1016/j.neuron.2008.09.014

Skaggs, W. E., McNaughton, B. L., Wilson, M. A., & Barnes, C. A. (1996). Theta phase precession in hippocampal neuronal populations and the compression of temporal sequences. *Hippocampus, 6,* 149–172. http://dx.doi.org/10.1002/(SICI)1098-1063(1996)6:2<149::AID-HIPO6>3.0.CO;2-K

Sławińskaab, U., & Kasicki, S. (1998). The frequency of rat's hippocampal theta rhythm is related to the speed of locomotion. *Brain Research, 796,* 327–331. http://dx.doi.org/10.1016/S0006-8993(98)00390-4

Smith, D. M., Barredo, J., & Mizumori, S. J. (2012). Complimentary roles of the hippocampus and retrosplenial cortex in behavioral context discrimination. *Hippocampus, 22,* 1121–1133. http://dx.doi.org/10.1002/hipo.20958

Sullivan, D., Csicsvari, J., Mizuseki, K., Montgomery, S., Diba, K., & Buzsáki, G. (2011). Relationships between hippocampal sharp waves, ripples, and fast gamma oscillation: Influence of dentate and entorhinal cortical activity. *The Journal of Neuroscience, 31,* 8605–8616. http://dx.doi.org/10.1523/JNEUROSCI.0294-11.2011

Talk, A., Kang, E., & Gabriel, M. (2004). Independent generation of theta rhythm in the hippocampus and posterior cingulate cortex. *Brain Research, 1015,* 15–24. http://dx.doi.org/10.1016/j.brainres.2004.04.051

Valenstein, E., Bowers, D., Verfaellie, M., Heilman, K. M., Day, A., & Watson, R. T. (1987). Retrosplenial amnesia. *Brain: A Journal of Neurology, 110,* 1631–1646. http://dx.doi.org/10.1093/brain/110.6.1631

Vanderwolf, C. H. (1969). Hippocampal electrical activity and voluntary movement in the rat. *Electroencephalography and Clinical Neurophysiology, 26,* 407–418. http://dx.doi.org/10.1016/0013-4694(69)90092-3

van Groen, T., & Wyss, J. M. (1990). Connections of the retrosplenial granular a cortex in the rat. *The Journal of Comparative Neurology, 300,* 593–606. http://dx.doi.org/10.1002/cne.903000412

van Groen, T., & Wyss, J. M. (1992). Connections of the retrosplenial dysgranular cortex in the rat. *The Journal of Comparative Neurology, 315,* 200–216. http://dx.doi.org/10.1002/cne.903150207

Van Groen, T., & Wyss, J. M. (2003). Connections of the retrosplenial granular b cortex in the rat. *The Journal of Comparative Neurology, 463,* 249–263. http://dx.doi.org/10.1002/cne.10757

Vann, S. D., & Aggleton, J. P. (2002). Extensive cytotoxic lesions of the rat retrosplenial cortex reveal consistent deficits on tasks that tax allocentric spatial memory. *Behavioral Neuroscience, 116,* 85–94. http://dx.doi.org/10.1037/0735-7044.116.1.85

Vann, S. D., & Aggleton, J. P. (2004). Testing the importance of the retrosplenial guidance system: Effects of different sized retrosplenial cortex lesions on heading direction and spatial working memory. *Behavioural Brain Research, 155,* 97–108. http://dx.doi.org/10.1016/j.bbr.2004.04.005

Vann, S. D., Aggleton, J. P., & Maguire, E. A. (2009). What does the retrosplenial cortex do? *Nature Reviews Neuroscience, 10,* 792–802. http://dx.doi.org/10.1038/nrn2733

Vann, S. D., Kristina Wilton, L. A., Muir, J. L., & Aggleton, J. P. (2003). Testing the importance of the caudal retrosplenial cortex for spatial memory in rats. *Behavioural Brain Research, 140,* 107–118. http://dx.doi.org/10.1016/S0166-4328(02)00274-7

Vedder, L. C., Miller, A. M., Harrison, M. B., & Smith, D. M. (2017). Retrosplenial cortical neurons encode navigational cues, trajectories and reward locations during goal directed navigation. *Cerebral Cortex, 27,* 3713–3723.

Vogt, B. A., & Miller, M. W. (1983). Cortical connections between rat cingulate cortex and visual, motor, and postsubicular cortices. *The Journal of Comparative Neurology, 216,* 192–210. http://dx.doi.org/10.1002/cne.902160207

Wang, D. V., & Ikemoto, S. (2016). Coordinated Interaction between hippocampal sharp-wave ripples and anterior cingulate unit activity. *The Journal of Neuroscience, 36,* 10663–10672. http://dx.doi.org/10.1523/JNEUROSCI.1042-16.2016

Whittington, M. A., Traub, R. D., Kopell, N., Ermentrout, B., & Buhl, E. H. (2000). Inhibition-based rhythms: Experimental and mathematical observations on network dynamics. *International Journal of Psychophysiology, 38,* 315–336. http://dx.doi.org/10.1016/S0167-8760(00)00173-2

Wilson, M. A., & McNaughton, B. L. (1993). Dynamics of the hippocampal ensemble code for space. *Science, 261,* 1055–1058. http://dx.doi.org/10.1126/science.8351520

Winson, J. (1974). Patterns of hippocampal theta rhythm in the freely moving rat. *Electroencephalography and Clinical Neurophysiology, 36,* 291–301. http://dx.doi.org/10.1016/0013-4694(74)90171-0

Wood, E. R., Dudchenko, P. A., Robitsek, R. J., & Eichenbaum, H. (2000). Hippocampal neurons encode information about different types of memory episodes occurring in the same location. *Neuron, 27,* 623–633. http://dx.doi.org/10.1016/S0896-6273(00)00071-4

Wyss, J. M., & Van Groen, T. (1992). Connections between the retrosplenial cortex and the hippocampal formation in the rat: A review. *Hippocampus, 2,* 1–11. http://dx.doi.org/10.1002/hipo.450020102

Yamawaki, N., Radulovic, J., & Shepherd, G. M. G. (2016). A corticocortical circuit directly links retrosplenial cortex to M2 in the mouse. *The Journal of Neuroscience, 36,* 9365–9374. http://dx.doi.org/10.1523/JNEUROSCI.1099-16.2016

Received January 11, 2018
Revision received April 20, 2018
Accepted May 1, 2018 ■